Metabolic imaging with the use of fluorescence lifetime imaging microscopy (FLIM) accurately detects mitochondrial dysfunction in mouse oocytes

Tim Sanchez, Ph.D.,[a] Tianren Wang, M.D., Ph.D.,[b] Marta Venturas Pedro, M.Sc.,[a] Man Zhang, M.D., Ph.D,[b] Ecem Esencan, M.D.,[b] Denny Sakkas, Ph.D.,[c] Dan Needleman, Ph.D.,[a] and Emre Seli, M.D.[b]

[a] Departments of Applied Physics and Molecular and Cellular Biology, Harvard University, Cambridge, Massachusetts; [b] Department of Obstetrics, Gynecology, and Reproductive Sciences, Yale University, New Haven, Connecticut; and [c] Boston IVF, Waltham, Massachusetts

Objective: To determine whether metabolic imaging with the use of fluorescence lifetime imaging microscopy (FLIM) identifies metabolic differences between normal oocytes and those with metabolic dysfunction.
Design: Experimental study.
Setting: Academic research laboratories.
Patient(s): None.
Intervention(s): Oocytes from mice with global knockout of *Clpp* (caseinolytic peptidase P; n = 52) were compared with wild-type (WT) oocytes (n = 55) as a model of severe oocyte dysfunction. Oocytes from old mice (1 year old; n = 29) were compared with oocytes from young mice (12 weeks old; n = 35) as a model of mild oocyte dysfunction.
Main Outcome Measure(s): FLIM was used to measure the naturally occurring nicotinamide adenine dinucleotide dehydrogenase (NADH) and flavin adenine dinucleotide (FAD) autofluorescence in individual oocytes. Eight metabolic parameters were obtained from each measurement (4 per fluorophore): short (τ_1) and long (τ_2) fluorescence lifetime, fluorescence intensity (*I*), and fraction of the molecule engaged with enzyme (*F*). Reactive oxygen species (ROS) levels and blastocyst development rates were measured to assess illumination safety.
Result(s): In *Clpp*-knockout oocytes compared with WT, FAD τ_1 and τ_2 were longer and *I* was higher, NADH τ_2 was longer, and *F* was lower. In old oocytes compared with young ones, FAD τ_1 was longer and *I* was lower, NADH τ_1 and τ_2 were shorter, and *I* and *F* were lower. FLIM did not affect ROS levels or blastocyst development rates.
Conclusion(s): FLIM parameters exhibit strong differentiation between *Clpp*-knockout versus WT, and old versus young oocytes. FLIM could potentially be used as a noninvasive tool to assess mitochondrial function in oocytes. (Fertil Steril® 2018;110:1387–97. ©2018 by American Society for Reproductive Medicine.)
El resumen está disponible en Español al final del artículo.

Key Words: Mitochondria, mitochondrial unfolded protein response, CLPP, oocyte, aging, fluorescence lifetime imaging microscopy, FLIM

Received May 23, 2018; revised July 24, 2018; accepted July 25, 2018.
T.S. is cofounder and a shareholder and officer of Luminova and coholds patent US20150346100A1 pending for metabolic imaging methods for assessment of oocytes and embryos and patent US20170039415A1 issued for nonlinear imaging systems and methods for assisted reproductive technologies. T.W. has nothing to disclose. M.V.P. has nothing to disclose. M.Z. has nothing to disclose. E.E. has nothing to disclose. D.S. is on the scientific advisory board of Cooper Surgical and has stock options with Luminova. D.N. is cofounder and a shareholder and officer of Luminova and coholds patent US20150346100A1 pending for metabolic imaging methods for assessment of oocytes and embryos and patent US20170039415A1 issued for nonlinear imaging systems and methods for assisted reproductive technologies. E.S. is a consultant and receives research funding from Foundation for Embryonic Competence.
Supported by the Blavatnik Biomedical Accelerator Grant at Harvard University, and by the Harvard Catalyst | The Harvard Clinical and Translational Science Center (National Institutes of Health Award UL1 TR001102). T.S. was supported by a National Science Foundation Postdoctoral Research Fellowship in Biology grant (1308878). T.W. was supported by the National Natural Science Foundation of China (81501247). E.S. was supported by award R01HD059909 from the National Institutes of Health.
Reprint requests: Emre Seli, M.D., 310 Cedar St., LSOG 304B, New Haven, CT 06520-8063 (E-mail: emre.seli@yale.edu).

Fertility and Sterility® Vol. 110, No. 7, December 2018 0015-0282/$36.00

https://doi.org/10.1016/j.fertnstert.2018.07.022

Developing a precise and reliable method of assessing oocyte and embryo quality has long been a critical goal for assisted reproductive technologies (ART) (1). Soon after the report of the first successful pregnancy with the use of in vitro fertilization (IVF) (2) and the introduction of controlled ovarian stimulation (3), embryo grading systems based on embryo morphology and cleavage rate were introduced (4–9). These approaches resulted in significant improvements in implantation and pregnancy rates (10), but their accuracy remained limited, with 60% of fresh embryos transferred to women younger than 35 years of age failing to implant (11). Implantation failure rate rises to 75% for women 41–42 years old, and to >80% for those who are 43–44 years old (11). Even in women undergoing IVF treatment with the use of fresh embryos generated with donor eggs, the implantation rate remains at 50% (11). These data are consistent with the observation that in many cases, embryos with acceptable morphology fail to implant because of underlying metabolic defects or chromosomal anomalies; conversely, many morphologically or morphokinetically irregular embryos are capable of producing healthy babies (12).

Aneuploidy is the most common type of chromosome abnormality and is the leading cause of implantation failure, miscarriage, and congenital abnormalities in humans (13–16). To improve the accuracy of embryo viability assessment, a number of investigators employed preimplantation genetic screening (now called preimplantation genetic testing for aneuploidy [PGT-A]) to diagnose embryo aneuploidy. Initial methods that used fluorescent in situ hybridization were later found not to be clinically useful (17). More recently, with the introduction of whole-genome amplification (WGA), combined with 24-chromosome polymerase chain reaction (PCR) or next-generation sequencing (NGS), along with efficient extended culture and embryo cryopreservation, a number of centers reached 65% sustained implantation rates and prospective randomized clinical trials demonstrated clinical benefits with the use of PGT-A (18, 19). Nevertheless, one-third of euploid embryos still fail to achieve sustained implantation, and it is likely that embryonic factors other than aneuploidy affect IVF success.

Mitochondrial function is essential for oocyte and embryo viability (20). More recently, methods have emerged to quantify mitochondrial DNA (mtDNA) copy number in trophectoderm biopsies taken for PGT-A (21). This approach has aimed to use mtDNA number as a reflection of overall mitochondrial function for embryos. Although some reports have indicated that especially high mtDNA counts are associated with poor embryo prognosis (21, 22), other reports have reported no such association (23, 24). Some have also proposed that the utility of this technique is intrinsically limited by a high level of natural variation in mtDNA levels (25).

Nicotinamide adenine dinucleotide (NAD+/NADH) and flavin adenine dinucleotide (FAD/$FADH_2$) are two cofactors that are involved in cellular respiration (26). They accept high-energy electrons that they transport to the electron transport chain (ETC), where the energy is used to generate adenosine triphosphate (ATP) molecules. When NAD+ and FAD accept electrons they are reduced to NADH (by receiving one proton [H+] and two electrons) and $FADH_2$ (by receiving two protons and two electrons), respectively. NADH molecules are formed during glycolysis (which does not require oxygen) in the cytoplasm, as well as during pyruvate decarboxylation into acetyl coenzyme A and in the Kreb cycle, both of which occur in the mitochondrial matrix. $FADH_2$ molecules are formed in the Kreb cycle. At perfect efficiency under aerobic conditions, a single glucose atom results in the generation of ten NADH and two $FADH_2$ molecules. NADH and $FADH_2$ are then oxidized at the ETC, located in the inner mitochondrial matrix, generating three and two ATPs per molecule, respectively (26).

In the present study, we evaluated the potential of fluorescence lifetime imaging microscopy (FLIM)–based metabolic imaging (27) of NADH and FAD as a tool for measuring mitochondrial metabolic state in oocytes for potential application in IVF. Because NADH and FAD are central to cellular respiration, differences in metabolic state directly affect measurable fluorescence properties of these molecules (28). In addition, these molecules are naturally fluorescent, avoiding the need for foreign probes or specialized reagents. We performed FLIM measurements with the use of time-correlated single photon counting (TCSPC) (29). FLIM via TCSPC uses fast electronics to record the subnanosecond arrival time of every photon in an image relative to the laser pulse that generated that photon. The analysis of these arrival times allows detailed information to be extracted about the fluorophores under study. Such approaches have been extensively used to characterize the metabolic state of cancer cells (30), other cell lines (31), stem cells (32), mammalian tissues (33), and germ cell differentiation in *Caenorhabditis elegans* (32). However, we are unaware of any studies using these advance methods on mammalian eggs and embryos.

With the use of two mouse models of mitochondrial dysfunction, we show that this technique is able to detect and quantitatively characterize known defects in mitochondrial function in oocytes. To investigate severe metabolic dysfunction, we used oocytes from mice with global germline deletion of the mitochondrial protease, *Clpp*. The deletion of this gene results in female infertility associated with severe mitochondrial dysfunction and metabolic abnormalities in oocytes (34). To investigate a milder form of metabolic dysfunction, we compared metabolic imaging measurements of oocytes from old and young mice. For each of these model systems, we compared the performance of FLIM with measurements of mtDNA amount. Finally, we performed an initial characterization of the safety of FLIM illumination. Given the intensity of light used for FLIM, the primary concern is the generation of reactive oxygen species (ROS) (35). We found that FLIM illumination of embryos resulted in no significant increase in ROS, and that it had no significant impact on blastocyst development rates.

MATERIALS AND METHODS

FLIM-Based Metabolic Imaging of NADH and FAD

FLIM measurements were performed on a Nikon microscope with the use of two-photon excitation from a Ti:Sapphire pulsed laser (M-Squared lasers) with an 80-MHz repetition

rate and ~150-fs pulse width, a galvanometer scanner, TCSPC module (SPC-150; Becker and Hickl) and a hybrid single-photon-counting detector (HPM-100-40; Becker and Hickl). The wavelength of excitation was set to 750 nm for NADH and 845 nm for FAD, with powers of 45 mW and 75 mW, respectively (measured after the objective). Optical bandpass filters were positioned in front of the detector: 460/50 nm for NADH and 550/88 nm for FAD (Chroma Technology). Imaging was performed with a 20× Nikon objective with 0.75 numeric aperture. The size of the equipment was similar to a typical microscope (with ~3 × 5 feet base area).

At each time point, NADH and FAD images were acquired at three different focal planes within the oocytes, separated by a distance of 7 μm, with an integration time of 60 seconds (11–12 integrated scans of the field of view) for each plane. Pixel size was 0.8 μm, and scanner dwell time was 5 μs/pixel. NADH/FAD complete acquisitions were orchestrated with a combination of custom software written in Labview and Becker Hickl acquisition software. In total, each complete metabolic measurement took ~7 minutes to acquire.

Mouse Breeding and Genotyping

We maintained the mice according to the Yale University animal research requirements. Food and water were available ad libitum and animals were housed under a 12-hour light-dark cycle. We obtained Institutional Animal Care and Use Committee approval before the initiation of the study (protocol number 2011-11207).

To obtain oocytes from old reproductive-age mice, we purchased 7-month-old C57BL/6J retired breeder female mice from Jackson Laboratories. For the "old" group, we killed mice at 12 months of age to retrieve oocytes. "Young" oocytes came from 12-week-old mice.

We acquired $Clpp^{+/-}$ male and female mice from the founder line IST13563G11 (line G) in the inbred C57BL/6J genetic background from Georg Auburger, Ph.D. (Goethe University Medical School) (36) and we bred them to obtain $Clpp^{-/-}$ (knockout) mice. The mouse genotyping was carried out as previously described (34).

Oocyte Collection

Mouse oocytes were collected with the use of standard protocols (37). Briefly, we superovulated female mice by means of intraperitoneal injection of 5 IU pregnant mare serum gonadotropin (PMSG; Sigma) to stimulate follicle development. We then killed the mice 44 hours later with the use of CO_2, removed the ovaries, and isolated cumulus oophorus complexes by puncturing the ovaries with the use of a 26.5-gauge needle under a dissecting microscope (Olympus SZH-ILLK). Cumulus cells were stripped with the use of 75 μm pipettes and germinal vesicle (GV) oocytes (arrested at the prophase of the first meiotic division) were collected.

Sample Preparation and FLIM Acquisition

Mouse oocytes were imaged in Vitrolife Primo Vision nine-well dishes with 330-μm-diameter microwells, with four oocytes per well. Each well contained one 50-μL droplet of α-minimum essential medium (MEMα; Life Technologies) supplemented with 20 mmol/L Hepes, 75 μg/mL penicillin G (Sigma), 50 μg/mL streptomycin sulfate (Sigma), 0.1% polyvinyl alcohol (Sigma), and 10 μmol/L milrinone (Sigma), covered with Vitrolife Ovoil paraffin oil. An on-stage incubator system (Ibidi) was used to keep oocytes at 37 ± 0.5°C during imaging. Oocytes were retrieved with a micropipette after metabolic imaging and frozen in separate tubes for subsequent mtDNA copy number measurements. During this process, correspondence was maintained so that metabolic measurements could be compared with mtDNA measurements in the same oocyte.

Quantification of mtDNA Copy Number in Oocytes

To quantify mtDNA levels in GV oocytes, the *Cox3* fragment was amplified and subcloned into pCR2.1-TOPO cloning vector (Invitrogen) as previously described (30). One Shot TOP10 Chemically Competent *Escherichia coli* were transformed and grown overnight at 37°C. Recombinant plasmids were purified with the use of the Qiagen plasmid isolation kit, and the inserted mtDNA fragment was confirmed by means of DNA sequence analysis. Plasmid DNA was quantified with the use of the Nanodrop 2000 spectrophotometer (Thermo Scientific). A standard curve from 10^8 to 10^1 plasmid molecules was generated by serial tenfold dilutions.

Individual GV oocytes were lysed in 10 μL lysis solution containing 125 μg/mL proteinase K and 17 μmol/L sodium dodecyl sulfate in sterile water by incubating at 55°C for 2 hours. Then proteinase K was inactivated by heating the lysis mix at 95°C for 10 minutes, and the mix was used directly for downstream PCR. Reactions were performed in triplicates. Each 10-μL reaction contained 5 μL Sybr Green Supermix (Bio-Rad Laboratories), ~0.3 μmol/L of each primer, and one-third of the total oocyte DNA. Oocyte mtDNA copy numbers were extrapolated from the standard curve.

FLIM Data Analyses

Data was analyzed with the use of custom Matlab code. For each of the three focal planes acquired at every time point, a machine-learning algorithm (based on the "Weka Segmentation" ImageJ plugin) was used on the intensity image to segment out the cytoplasmic region of each oocyte. Photons collected from the oocyte at the three focal planes were combined together into a single photon arrival histogram. The resulting histogram was fit to a sum of two exponentials:

$$P(t) = A[F\exp(-t/\tau_1) + (1-F)\exp(-t/\tau_2)] + B$$

Here, A is a normalization factor, F is the fraction of fluorophores with lifetime τ_1, the remaining fluorophores $(1-F)$ having a lifetime of τ_2, and B is a background term (not coming from the fluorophore of interest). Overall fluorophore intensity, I, is additionally obtained by adding up all photons detected within an oocyte and dividing by the oocyte area and number of integrated scans. Fits were performed for both NADH and FAD, providing a total of eight quantitative parameters for characterizing the metabolic state of each oocyte: I, F, τ_1, and τ_2, for both NADH and FAD.

Repeated measurements on the same oocytes over a 70-minute period revealed small decreases in measured metabolic parameters over time (fractions engaged <1%, τ_2's <2%, intensities <8%, τ_1's <22%). Linear regression of this data was used to calibrate and correct for this time variation in subsequent measurements. Performing this correction produced quantitative changes in the metabolic parameters, but did not qualitatively influence the conclusions of the study.

Kolmogorov-Smirnov tests were performed on group distributions for each individual parameter to determine distribution normality. Student *t* tests were performed between groups for each individual parameter, taking $P<.05$ to be statistically significant. In the *Clpp* experiment, we also derived a test condition by using a support machine vector algorithm. This method uses the data sets to calculate a hyperplane that optimally separates the two data sets, 55 $Clpp^{+/+}$ and 52 $Clpp^{-/-}$ oocytes. Data points were deemed to be positive or negative based on whether they lay above or below the hyperplane.

Reactive Oxygen Species, Blastocyst Development, and Calculating Light Absorption

Groups of embryos were incubated on the microscope and subjected to the following varying degrees of FLIM illumination: 1 metabolic measurement, 3 measurements (1 per day), 24 measurements (1 every 2 hours), and 44 measurements (1 every 2 hours). For groups receiving 1, 3, and 24 measurements, we used CD1 embryos frozen at the 2-cell stage. The 44-measurement group entailed a longer incubation (88 hours), so we used a different strain of embryos (B6C3F1 female + B6D2F1 male) that were frozen at the 1-cell stage. All embryos for these safety experiments were purchased from Embryotech. ROS measurements at the blastocyst stage and blastocyst development rates were subsequently measured. For each experiment, measurements of illuminated embryos were compared with control groups of embryos incubated in the same dish but receiving no illumination.

For ROS studies, embryos were stained at blastocyst stage with an ROS reporter dye, HC-DCFDA (Sigma 7722-84-1). Staining was performed according to Sigma's provided protocol, incubating embryos in MEMα containing 25 μmol/L HC-DCFDA for 15 minutes. Embryos were then transferred to MEMα medium, and HC-DCFDA fluorescence was imaged with the use of 900 nm illumination and a 550/88 nm emission filter. One ROS measurement was generated for each blastocyst by calculating the total photons within the intracellular region and dividing by the intracellular area to get an average intensity value. Autofluorescence from FAD was measured before staining with the same imaging conditions, and the average autofluorescence was subtracted from ROS values for each group.

Blastocyst development rates were recorded for all embryo groups. Illuminated embryo rates were compared with nonilluminated embryos grown on the microscope, as well as with embryos cultured in a table-top incubator (Panasonic MCO5MPA).

We also performed physical calculations to estimate the amount of light energy absorbed by FAD in an oocyte during an FAD FLIM acquisition. We first derived an estimate from first principles, considering one- and two-photon absorption cross-sections, absorption due to pulsed illumination, confocal volume, and other factors (38). We then performed a corroborating empirical estimate, deriving absorbed energy from our measured photon counts. These values were then compared with similar estimates of energy absorbed during a standard morphologic assessment with the use of brightfield microscopy.

RESULTS

$Clpp^{-/-}$ versus $Clpp^{+/+}$ Oocytes

We first tested the hypothesis that FLIM-based metabolic imaging can accurately detect severe metabolic dysfunction in oocytes by studying $Clpp^{+/+}$ (wild-type) and $Clpp^{-/-}$ (knockout) oocytes. We imaged a total of 55 $Clpp^{+/+}$ oocytes and 52 $Clpp^{-/-}$ oocytes, four at a time, in microwells. For each microwell, we obtained FLIM data on NADH and FAD, segmented out the individual oocytes with the use of the intensity images, fit the oocytes histogram of photon arrival times with the use of a model, and obtained a total of eight metabolic parameters: fluorescence intensity (*I*), short lifetime (τ_1), long lifetime (τ_2), and fraction engaged with enzyme (*F*), for both NADH and FAD (Fig. 1). Thus, FLIM of NADH and FAD provided both subcellular morphologic information and a quantitative characterization of mitochondrial metabolism.

We first compared the morphology of $Clpp^{+/+}$ and $Clpp^{-/-}$ oocytes. Although brightfield images of $Clpp^{+/+}$ and $Clpp^{-/-}$ oocytes appeared quite similar (compare left-hand images of Fig. 2A and 2B), the NADH intensity images were markedly different, with many $Clpp^{-/-}$ oocytes displaying a strong NADH signal around their periphery (compare righthand images of Fig. 2A and 2B). Because NADH is highly enriched in mitochondria (39), the brighter regions of the NADH images reflect the concentration of mitochondria, indicating that the subcellular localization of mitochondria is often perturbed in $Clpp^{-/-}$ oocytes. Conversely, $Clpp^{+/+}$ oocytes did not exhibit such mitochondrial anomalies, and consistently showed perinuclear localization of the mitochondria, which has been previously observed to occur during oocyte maturation (40, 41). We therefore concluded that NADH imaging of oocytes provides novel morphologic information that is inaccessible to conventional brightfield microscopy.

We next investigated biochemical differences between mitochondria in $Clpp^{-/-}$ and $Clpp^{+/+}$ oocytes. Five of the eight measured FLIM parameters revealed extremely significant differences between $Clpp^{+/+}$ and $Clpp^{-/-}$ oocytes (Fig. 2C): NADH τ_2 (P=1.4e−27), FAD τ_2 (P=6e−28), NADH *F* (P=6e−27), FAD *I* (P=3e−8), and FAD τ_1 (P=3e−3). The support vector machine calculation performed on the three most differentiating parameters (NADH τ_2, FAD τ_2, and NADH *F*) produced a plane that perfectly separated the data, producing a test sensitivity and specificity of 1 (Fig. 2D), demonstrating that the differences in their metabolism can be easily resolved with FLIM.

FIGURE 1

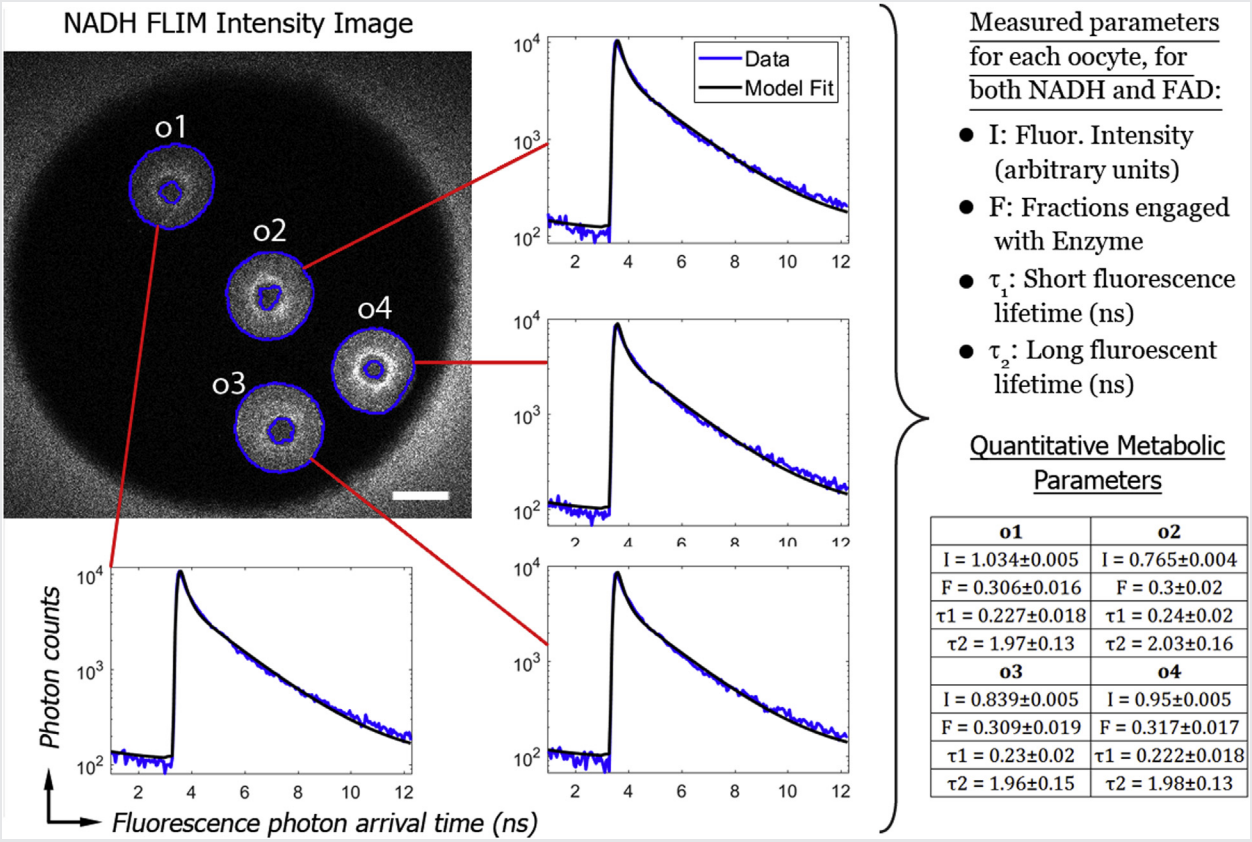

Dinucleotide dehydrogenase (NADH) intensity image of four *Clpp*$^{+/+}$ (wild-type) oocytes in one microwell of a 9-well dish. The cytoplasm of the oocytes was segmented (*blue line boundaries*), and oocytes were individually identified (here labeled *o1*, *o2*, *o3*, and *o4*). Scale bar = 50 μm. Histograms of photon counts versus fluorescence photon arrival time were constructed for each oocyte (*blue lines*) and fitted with a model containing two fluorescent species (*black lines*). These fits allow four parameters to be measured. Similar fits were also performed for flavin adenine dinucleotide (FAD) fluorescence, allowing an additional four parameters to be measured. Parameter values are displayed with 95% confidence intervals.

Sanchez. FLIM detects mitochondrial dysfunction. Fertil Steril 2018.

In contrast, comparing mtDNA copy number, measured by quantitative reverse-transcription (qRT) PCR, revealed only a marginally significant difference between *Clpp*$^{-/-}$ and *Clpp*$^{+/+}$ oocytes (P=.042; Fig. 2E). Because mtDNA measurements were taken on the same oocytes as the FLIM measurements, we were able to investigate the correlation between them. However, we did not observe strong correlations between FLIM parameters and mtDNA. NADH τ_1 showed the highest correlation, with a Pearson coefficient of only 0.34.

Old Versus Young Oocytes

We next compared oocytes from old and young mothers to determine whether FLIM-based metabolic imaging can detect mild metabolic dysfunction. We imaged a total of 29 oocytes from old (1-year-old) mice and 35 oocytes from young (12-week-old) mice. Neither brightfield images nor NADH intensity images revealed obvious differences between the morphology of young and old oocytes (Fig. 3A and 3B). In contrast, four of the eight measured FLIM parameters were highly significantly different between young and old oocytes (Fig. 3C): NADH τ_1 (P=2.7e−6), NADH τ_2 (P=9e−4), NADH I (P=3e−3), and NADH F (P=.02). Simultaneously plotting the NADH τ_1, NADH τ_2, NADH I, for each oocyte on one three-dimensional graph revealed a clear separation between young and old oocytes (Fig. 3D). Sensitivity or specificity was not calculated, however, because age is not a disease condition, but rather only correlates with oocyte failure.

In contrast to our findings with the use of FLIM, mtDNA copy number was not significantly different between young and old oocytes (P=.14) (Fig. 3E). We also found no significant correlation between mtDNA and any of the FLIM parameters (the highest Pearson correlation coefficient measured was 0.1 for FAD F).

Safety of FLIM Illumination

We observed no significant difference in ROS levels between illuminated and nonilluminated embryos for any of the administered photodoses (Fig. 4A). Embryo numbers for the photodoses were: for 1 measurement, n = 33 illuminated

FIGURE 2

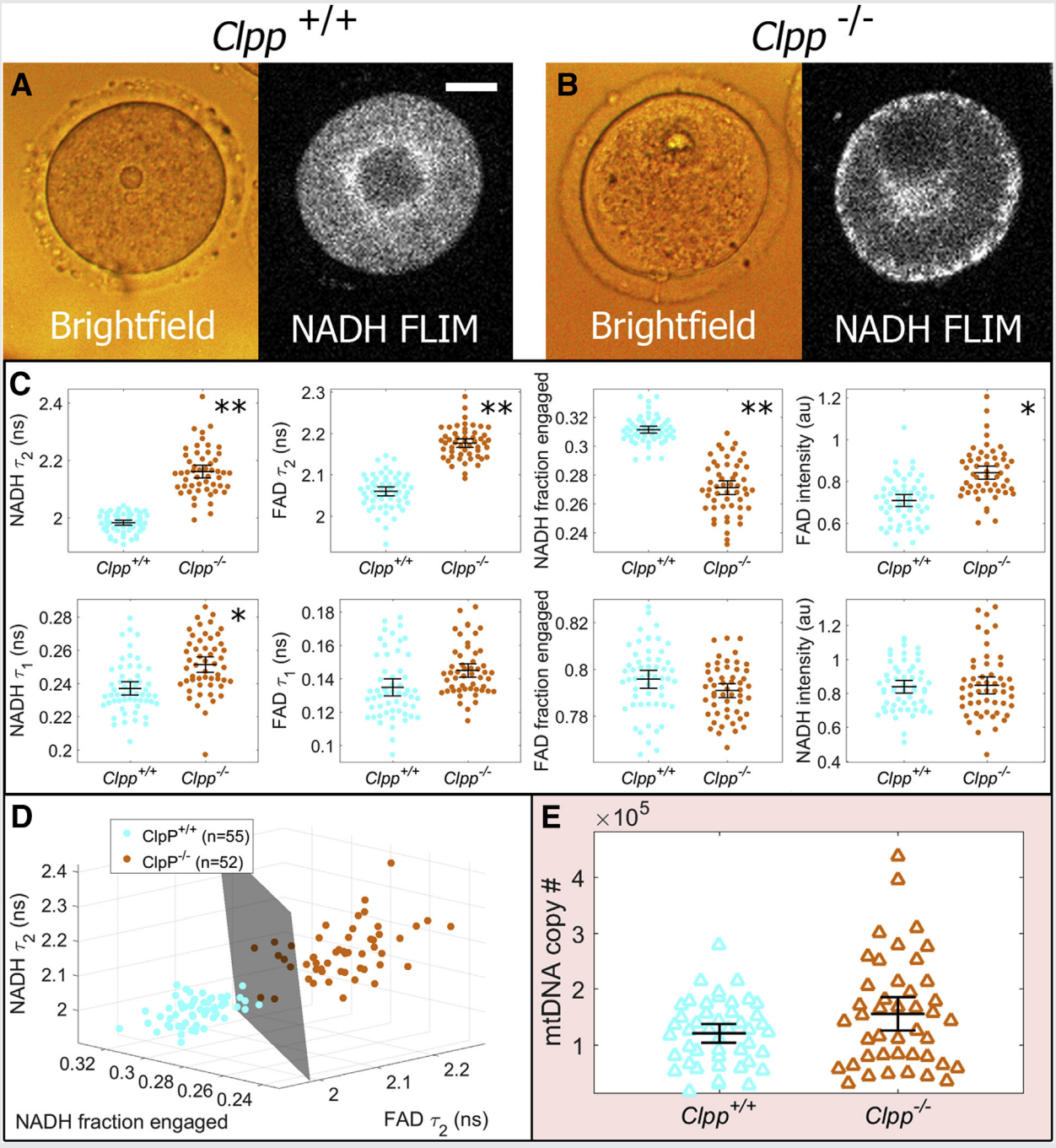

Comparative assessments of *Clpp*$^{+/+}$ and *Clpp*$^{-/-}$ oocytes. **(A)** Brightfield images show gross morphologic features of oocytes, although NADH FLIM intensity images reflect the mitochondrial distribution. **(B)** Obvious defects in *Clpp*$^{-/-}$ oocytes were not observed in brightfield images, but fluorescence imaging revealed aberrant mitochondrial distributions in many oocytes. **(C)** Metabolic imaging of *Clpp*$^{+/+}$ (n = 55) and *Clpp*$^{-/-}$ (n = 52) oocytes detected highly significant differences in five of the eight parameters measured. Parameters are plotted in order of decreasing separation. (*P<.005; **P<10^{-26}) **(D)** If the three most sensitive metabolic parameters (NADH long lifetime [τ_2], NADH fraction engaged, and FAD τ_2) are represented in a three-dimensional plot, we can fit a plane that perfectly separates the two data sets. **(E)** *Clpp*$^{+/+}$ (n = 46) and *Clpp*$^{-/-}$ (n = 43) oocytes were lysed to obtain individual mtDNA copy number measurements. Student t tests on mtDNA measurements showed only a marginally significant difference (P=.042). Error bars represent 95% confidence intervals. FLIM = fluorescence lifetime imaging microscopy; other abbreviations as in Figure 1.

Sanchez. FLIM detects mitochondrial dysfunction. Fertil Steril 2018.

FIGURE 3

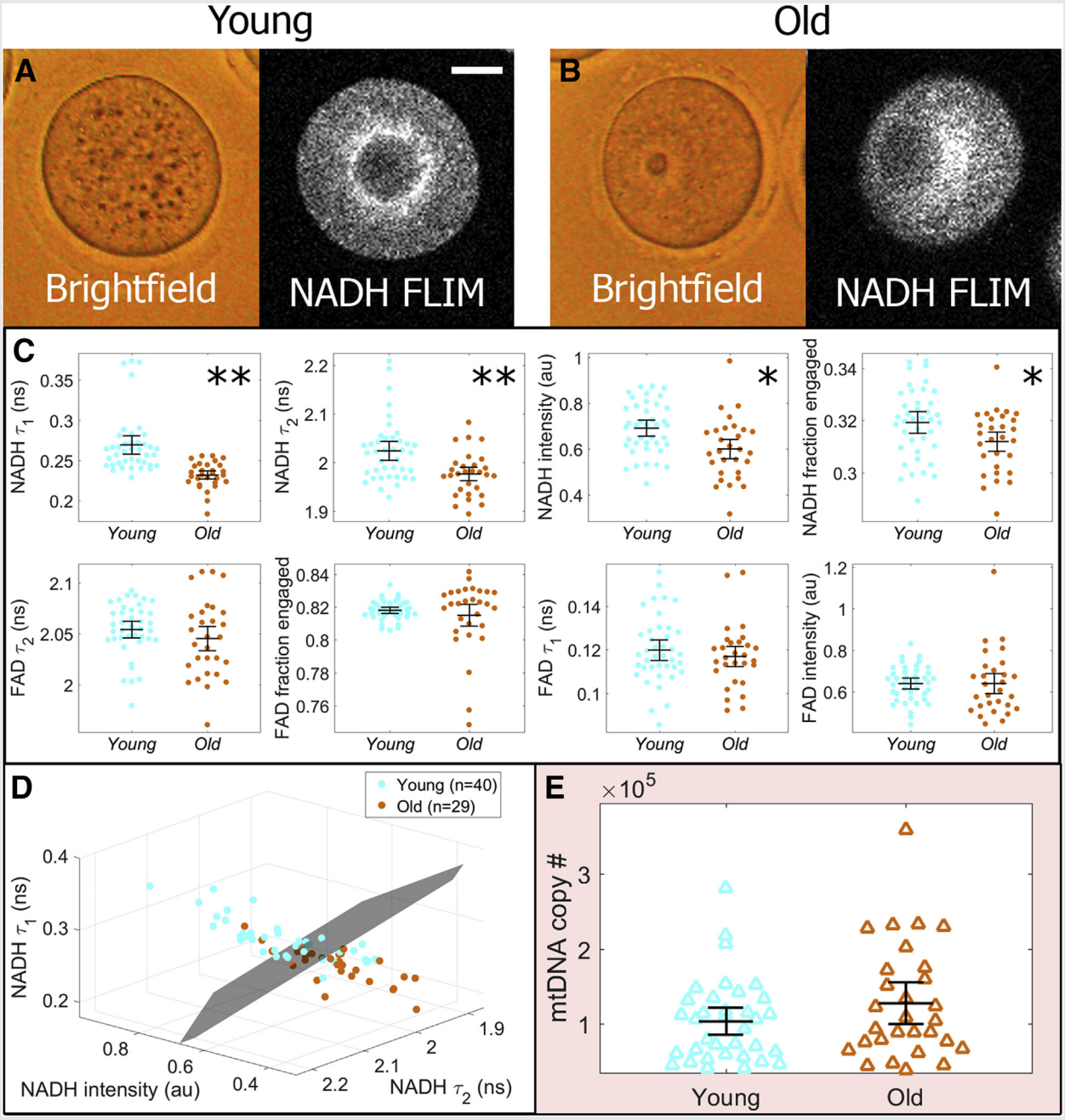

Comparative assessments of oocytes from old (12-month-old) and young (12-week-old) mice. **(A, B)** Neither brightfield images nor FLIM intensity images revealed obvious differences in morphology or mitochondrial distribution. Scale bar = 20 μm. **(C)** Conversely, metabolic imaging measurements on the same oocytes effectively differentiated young (n = 40) and old (n = 29) groups, with four of the eight parameters showing significant differences. Parameters are plotted in order of decreasing separation. *P<.03; **P<10^{-3}). P values were not as low as with *Clpp* wild-type versus knockout, the more severe case of metabolic dysfunction. **(D)** If the three most sensitive metabolic parameters (NADH intensity, NADH short lifetime [τ_1], and NADH τ_2) are represented in a three-dimensional plot, we can draw a plane that effectively separates the two data sets; however, there is more overlap between the distributions than in the more extreme case of *Clpp* knockout versus wild-type. **(E)** mtDNA copy number measurements were taken on young (n = 35) and old (n = 29) oocytes, and no significant difference between the two groups was observed (P=.14). Error bars represent 95% confidence intervals. Abbreviations as in Figures 1 and 2.

Sanchez. FLIM detects mitochondrial dysfunction. Fertil Steril 2018.

FIGURE 4

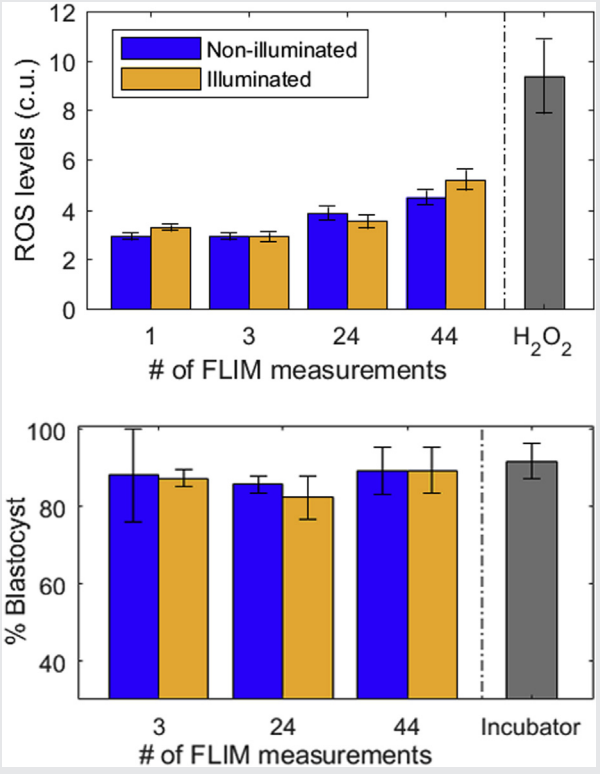

Evaluation of safety for varying photodoses of fluorescence lifetime imaging microscopy (FLIM) illumination. *Top*: Reactive oxygen species (ROS) levels were measured via HC-DCFDA fluorescence (custom units). Significant differences between illuminated and nonilluminated embryos were not observed for any of the photodoses studied. Embryos exposed to 30 mmol/L H_2O_2 were measured as positive control. Standard error bars represent variation between individual embryo measurements. *Bottom*: Embryos were cultured on the microscope, and blastocyst development rates of illuminated embryos were compared with nonilluminated embryos in the same dish. Embryos cultured in a standard incubator were used as a control. FLIM illumination did not have any significant impact on blastocyst development rates. Standard error bars represent variation between experiment batches.

Sanchez. FLIM detects mitochondrial dysfunction. Fertil Steril 2018.

and n = 33 nonilluminated embryos; for 3 measurements, n = 33 illuminated and n = 33 nonilluminated embryos; for 24 measurements, n = 18 illuminated and n = 18 nonilluminated embryos; and for 44 measurements, n = 37 illuminated and n = 39 nonilluminated embryos.

FLIM illumination resulted in no measurable impact on blastocyst development rates (Fig. 4B). For each photodose, blastocyst rates were averaged between several replicates with the following numbers: for 3 measurements, n = 39 illuminated and n = 37 nonilluminated batches; for 24 measurements, n = 184 illuminated and n = 205 nonilluminated batches; and for 44 measurements, n = 52 illuminated and n = 51 nonilluminated batches.

Theoretical estimates of light energy absorbed during an FAD FLIM acquisitions yielded values of 1.75 pJ from first principles and 2.31 pJ from our empirical estimate. In comparison, we estimate that oocytes absorb 2.62 pJ light energy during 10 seconds of a standard morphologic assessment.

DISCUSSION

We report the application of FLIM-based metabolic imaging of NADH and FAD as a diagnostic strategy for identifying metabolic dysfunction in oocytes. To adequately assess the diagnostic potential of FLIM, we used two models. First, we compared mice with a targeted deletion of *Clpp* with wild-type mice. *Clpp* is a key factor in mitochondrial stress response, and its absence is associated with impaired mitochondrial function and loss of mitochondrial protein homeostasis (proteostasis), therefore generating a severe metabolic dysfunction (34). In addition, *Clpp*-knockout mice display elevated mtDNA copy number and infertility. The second model compared oocytes from young (12-week-old) and old (1-year-old) mice providing an example of mild/moderate metabolic dysfunction, as previously published (42).

Metabolic imaging parameters exhibited clear separations between control and test groups for both old versus young and *Clpp* knockout versus wild-type experiments. Aging resulted in decreased NADH *I*, which is in agreement with previous studies showing decreasing NADH levels in various cell types (43). Old oocytes also had lower NADH *F*, NADH τ_2 and τ_1, and FAD τ_2. Group separation was not as large as in the *Clpp*-deficient oocytes, consistent with the premise that aging is not as severe as a metabolic mutation, and there was significant overlap in the old and young parameter distributions. This observation is in agreement with what is known to be true in the clinical context—that young mothers have more viable eggs than old mothers on average, but young mothers have some nonviable eggs and old mothers have some viable ones.

Knockout of *Clpp* resulted in different parameter shifts: higher FAD *I*, higher FAD τ_2 and τ_1, and lower NADH *F*. This difference in metabolic signature is not surprising, because these two types of metabolic dysfunction are likely due to very distinct mechanisms. Furthermore, the overall distributions of the two different strains were very different, indicating strain dependence of metabolic states. This intriguing result suggests that "healthy" metabolic function can be achieved via multiple metabolic configurations in different systems. For clinical diagnostic purposes, it is sufficient to show that within systems, this technique has high precision for differentiating metabolic states associated with good and bad prognosis. In humans, we may expect that healthy metabolism would have consistent parameter ranges, and that various forms of metabolic defects would register as deviations from these "Goldilocks" ranges (44).

At this early stage, we can make several first-order physiologic interpretations of the data. Intensity changes primarily reflect changes in molecule concentrations, and fractions engaged provide information about enzyme activity. Changes in NADH τ_2 and FAD τ_1 (engaged lifetimes) can be caused by a change in the proportions of molecules engaged with different kinds of enzymes. To make more precise interpretations, experiments using controlled metabolic perturbations and biophysical modeling are underway.

We found that the differences observed between the groups regarding FLIM parameters were much more significant compared with those achieved by mtDNA quantification. mtDNA copy number was significantly different between *Clpp*-knockout mouse oocytes compared with oocytes obtained from same-age wild-type mice ($P<.05$), whereas the mtDNA copy number of old and young mouse GV-stage oocytes did not differ. Several factors could explain the limitations of mtDNA copy number as a diagnostic test. First, significant variation in mtDNA copy number exists between individual oocytes. Indeed, in both mice and humans, 50,000–550,000 mtDNA copies are found in oocytes, with considerable degree of variability between samples and with increasing variability with age in humans (45–49). Our observations in the present study are consistent with previous reports on this subject. Second, mtDNA copy number measurement in a single cell (or 5 to 10 cells available in a trophoectoderm biopsy) is challenging owing to low copy number. Investigators tackled this issue using different techniques. Some used qRT-PCR followed by normalization to Alu repeat sequences in nuclear DNA (21). Others measured mtDNA copy number by NGS normalized to total nuclear DNA following WGA (24), and we performed absolute quantification by cloning a segment of mtDNA and using known copy number as standard (42). While each one of these approaches is justified scientifically, the level of intra- and interassay variability that they introduce remains to be established. Finally, mtDNA copy number is an indirect marker of cellular distress, because there are currently no experimental models showing a direct correlation (linear or otherwise) between cellular stress and mtDNA copy number. Although targeted deletion of genes required for key mitochondrial functions have been associated with elevated mtDNA copy number (34), others have reported low mtDNA copy number in nonhuman animal models of mitochondrial distress (50). These challenges contribute to the current debate regarding the use of mtDNA copy number in embryo viability assessment. Initial studies from two independent groups strongly suggested that mtDNA copy number is higher in euploid embryos that fail to implant (22, 36). The findings of those two studies have been challenged by others who failed to find a similar association (23) and a recent report showing that higher mtDNA copy number did not predict implantation failure in sibling embryos (in women undergoing double-embryo transfer) (24).

Although the present findings regarding the use of FLIM for metabolic imaging of oocytes findings are quite promising, our study has a number of limitations. First, we used a mouse model, which allowed us to conduct our experiments in a genetically homogeneous system. Although the level of variations in humans remains to be determined through clinical studies, it is likely that mitochondrial states will not be much more heterogeneous in humans, because mitochondrial state and function are under tight selective pressure. Second, we assessed FLIM parameters in GV-stage oocytes, primarily because *Clpp* knockout mice generate low numbers of mature oocytes or early embryos, and assessment at the GV stage allowed us to compare and contrast the two models. Whether metabolic distress in embryos results in similar deviations from normal remains to be investigated. Finally, and most importantly, the present study demonstrates a clear distinction only between healthy and unhealthy cohorts (wild type vs. *Clpp* knockout and young vs. old). Although these findings are promising, whether FLIM parameters will be able to differentiate embryos that are "more" or "less" likely to implant within the same cohort (i.e., embryos obtained from the same patient) will be important to investigate.

The discovery of biomarkers for human embryo viability is a central challenge for contemporary reproductive scientists. Our findings, combined with recently reported correlations between mtDNA copy number and human embryo viability, suggest that mitochondrial metabolic parameters may play a role in determining the viability of oocytes and potentially the implantation potential of euploid embryos. Further research is required to validate the accuracy and clinical potential of this test.

Acknowledgments: The authors thank Becker and Hickl for contributing a single-photon-counting detector and TCSPC electronics to this research.

REFERENCES

1. Bromer JG, Seli E. Assessment of embryo viability in assisted reproductive technologies: shortcomings of current approaches and the emerging role of metabolomics. Curr Opin Obstet Gynecol 2008;20:234–41.
2. Steptoe PC, Edwards RG. Birth after the reimplantation of a human embryo. Lancet 1978;2:366.
3. Trounson A, Leeton J, Wood C, Webb J, Wood J. Pregnancies in humans by fertilization in vitro and embryo transfer in the controlled ovulatory cycle. Science 1981;216:681–2.
4. Scott LA, Smith S. The successful use of pronuclear embryo transfer the day following oocyte retrieval. Hum Reprod 1998;13:1003–13.
5. Tesarik J, Greco E. The probability of abnormal preimplantation development can be predicted by a single static observation on pronuclear state morphology. Hum Reprod 1999;14:1318–23.
6. Veeck L. An atlas of human gametes and conceptuses: an illustrated reference for assisted reproductive technology. New York: Parthenon; 1999.
7. Gerris J, de Neubourg D, Mangelschots K, Van Royen E, Van de Meerssche M, Valkenburg M. Prevention of twin pregnancy after in-vitro fertilization or intracytoplasmic sperm injection based on strict embryo criteria: a prospective randomized clinical trial. Hum Reprod 1999;14:2581–7.
8. VanRoyan E, Mangelschots K, de Neubourg D, Valkenburg M, van de Meerssche M, Ryckaert G, et al. Characterization of a top quality embryo, a step toward single-embryo transfer. Hum Reprod 1999;14:2345–9.
9. Gardner DK, Schoolcraft WB. In vitro culture of human blastocysts. In: Jansen R, Mortimer D, editors. Toward reproductive certainty: fertility and genetics beyond. Carnforth: Parthenon; 1999:378–88.
10. Toner JP. Progress we can be proud of: U.S. trends in assisted reproduction over the first 20 years. Fertil Steril 2002;78:943–50.
11. Society for Assisted Reproductive Technology. Assisted reproductive technology success rates. National summary and fertility clinic reports. Centers for Disease Control and Prevention; 2013. Available at: https://www.cdc.gov/art/pdf/2013-report/art-2013-fertility-clinic-report.pdf. Accessed March 10, 2018.
12. Stecher A, Vanderzwalmen P, Zintz M, Wirleitner B, Schuff M, Spitzer D, et al. Transfer of blastocysts with deviant morphological and morphokinetic parameters at early stages of in-vitro development: a case series. Reprod Biomed Online 2014;28:424–35.
13. Hassold T, Abruzzo M, Adkins K, Griffin D, Merrill M, Millie E, et al. Human aneuploidy: incidence, origin, and etiology. Environ Mol Mutagen 1996;28:167–75.

14. Hassold T, Chiu D. Maternal age–specific rates of numerical chromosome abnormalities with special reference to trisomy. Hum Genet 1985;70:11–7.
15. Hassold T, Hall H, Hunt P. The origin of human aneuploidy: where we have been, where we are going. Hum Mol Genet 2007;16:R203–8.
16. Hassold T, Hunt P. To err (meiotically) is human: the genesis of human aneuploidy. Nat Rev Genet 2001;2:280–91.
17. Mastenbroek S, Twisk M, van der Veen F, Repping S. Preimplantation genetic screening: a systematic review and meta-analysis of RCTs. Hum Reprod Update 2011;17:454–66.
18. Scott RT, Upham KM, Forman EJ, Hong KH, Scott KL, Taylor D, et al. Blastocyst biopsy with comprehensive chromosome screening and fresh embryo transfer significantly increases in vitro fertilization implantation and delivery rates: a randomized controlled trial. Fertil Steril 2013;100:697–703.
19. Forman EJ, Hong KH, Ferry KM, Tao X, Taylor D, Levy B, et al. In vitro fertilization with single euploid blastocyst transfer: A randomized controlled trial. Fertil Steril 2013;100:100–7.
20. Seli E. Mitochondrial DNA as a biomarker for in-vitro fertilization outcome. Curr Opin Obstet Gynecol 2016;28:158–63.
21. Fragouli E, Spath K, Alfarawati S, Kaper F, Craig A, Michel CE, et al. Altered levels of mitochondrial DNA are associated with female age, aneuploidy, and provide an independent measure of embryonic implantation potential. PLoS Genet 2015;11:e1005241.
22. Diez-Juan A, Rubio C, Marin C, Martinez S, Al-Asmar N, Riboldi M, et al. Mitochondrial DNA content as a viability score in human euploid embryos: less is better. Fertil Steril 2015;104:534–41.
23. Victor AR, Brake AJ, Tyndall JC, Griffin DK, Zouves CG, Barnes FL, et al. Accurate quantitation of mitochondrial DNA reveals uniform levels in human blastocysts irrespective of ploidy, age, or implantation potential. Fertil Steril 2017;107:34–42.
24. Treff NR, Zhan Y, Tao X, Olcha M, Han M, Rajchel J, et al. Levels of trophectoderm mitochondrial DNA do not predict the reproductive potential of sibling embryos. Hum Reprod 2017;32:954–62.
25. Hicks KA, Howe DK, Leung A, Denver DR, Estes S. In vivo quantification reveals extensive natural variation in mitochondrial form and function in *Caenorhabditis briggsae*. PLoS One 2012;7:e43837.
26. Scott R, Zhang M, Seli E. Metabolism of the oocyte and the preimplantation embryo: implications for assisted reproduction. Curr Opin Obstet Gynecol 2018;30:163–70.
27. Becker W. Fluorescence lifetime imaging–techniques and applications. J Microsc 2012;247:119–36.
28. Heikal A. Intracellular coenzymes as natural biomarkers for metabolic activities and mitochondrial anomalies. Biomark Med 2010;4:241–63.
29. Becker W. Advanced time-correlated single photon counting techniques. Berlin and Heidelberg: Springer-Verlag; 2005.
30. Yu Q, Heikal A. Two-photon autofluorescence dynamics imaging reveals sensitivity of intracellular NADH concentration and conformation to cell physiology at the single-cell level. J Photochem Photobiol B 2009;95:46–57.
31. Niesner R, Peker B, Schlüsche P, Gericke K-H. Noniterative biexponential fluorescence lifetime imaging in the investigation of cellular metabolism by means of NAD(P)H autofluorescence. Chemphyschem 2004;5:1141–9.
32. Stringari C, Cinquin A, Cinquin O, Digman MA, Donovan PJ, Gratton E. Phasor approach to fluorescence lifetime microscopy distinguishes different metabolic states of germ cells in a live tissue. Proc Natl Acad Sci U S A 2011;108:13582–7.
33. Skala M, Riching K, Bird D, Gendron-Fitzpatrick A, Eickhoff J, Eliceiri K, et al. In vivo multiphoton fluorescence lifetime imaging of protein-bound and free nicotinamide adenine dinucleotide in normal and precancerous epithelia. J Biomed Opt 2007;12:24014.
34. Wang T, Babayev E, Jiang Z, Li G, Zhang M, Esencan E, et al. Mitochondrial unfolded protein response gene *Clpp* is required to maintain ovarian follicular reserve during aging, for oocyte competence, and development of preimplantation embryos. Aging Cell. In press.
35. Masters BR, So P. Handbook of biomedical nonlinear optical microscopy. Oxford University Press; 2008.
36. Gispert S, Parganlija D, Klinkenberg M, Dröse S, Wittig I, Mittelbronn M, et al. Loss of mitochondrial peptidase Clpp leads to infertility, hearing loss plus growth retardation via accumulation of CLPX, mtDNA and inflammatory factors. Hum Mol Genet 2013;22:4871–87.
37. Seli E, Lalioti MD, Flaherty SM, Sakkas D, Terzi N, Steitz JA. An embryonic poly(A)-binding protein (ePAB) is expressed in mouse oocytes and early preimplantation embryos. Proc Natl Acad Sci U S A 2005;102:367–72.
38. Denk W, Strickler JH, Webb WW. Two-photon laser scanning fluorescence microscopy. Science 1990;248:73–6.
39. Stein L, Imai S. The dynamic regulation of NAD metabolism in mitochondria. Trends Endocrinol Metab 2012;23:420–8.
40. Van Blerkom J, Runner M. Mitochondrial reorganization during resumption of arrested meiosis in the mouse oocyte. Am J Anat 1984;171:335–55.
41. Muggleton-Harris A, Brown J. Cytoplasmic factors influence mitochondrial reorganization and resumption of cleavage during culture of early mouse embryos. Hum Reprod 1988;3:1020–8.
42. Babayev E, Wang T, Lowther K, Horvath T, Taylor HS, Seli E. Aging is associated with changes in mitochondrial dynamics, function and mtDNA quantity. Maturitas 2016;93:121–30.
43. Camacho-Pereira J, Tarragó MG, Chini CCS, Nin V, Escande C, Warner GM, et al. CD38 dictates age-related NAD Decline and mitochondrial dysfunction through an SIRT3-dependent mechanism. Cell Metab 2016;23:1127–39.
44. Leese HJ, Guerif F, Allgar V, Brison DR, Lundin K, Sturmey RG. Biological optimization, the Goldilocks principle, and how much is lagom in the preimplantation embryo. Mol Reprod Dev 2016;83:748–54.
45. Steuerwald N, Barritt JA, Adler R, Malter H, Schimmel T, Cohen J, et al. Quantification of mtDNA in single oocytes, polar bodies and subcellular components by real-time rapid cycle fluorescence monitored PCR. Zygote 2000;8:209–15.
46. Reynier P, May-Panloup P, Chrétien MF, Morgan CJ, Jean M, Savagner F, et al. Mitochondrial DNA content affects the fertilizability of human oocytes. Mol Hum Reprod 2001;7:425–9.
47. Chen X, Prosser R, Simonetti S, Sadlock J, Jagiello G, Schon EA. Rearranged mitochondrial genomes are present in human oocytes. Am J Hum Genet 1995;57:239–47.
48. Pikó L, Taylor KD. Amounts of mitochondrial DNA and abundance of some mitochondrial gene transcripts in early mouse embryos. Dev Biol 1987;123:364–74.
49. Chan CC, Liu VW, Lau EY, Yeung WS, Ng EH, Ho PC. Mitochondrial DNA content and 4977 bp deletion in unfertilized oocytes. Mol Hum Reprod 2005;11:843–6.
50. Zhang M, Wang T, Esencen E, Jiang Z, Seli E. Disruption mitofusin 1 in oocyte results in defective ovarian follicle development and female infertility [abstract]. In: 65th Annual Scientific Meeting of the Society for Reproductive Investigation; 2018 March; San Diego, CA. Reproductive Sciences; 2018 March. Abstract O-155.

La imagen metabólica mediante el uso de la microscopia de fluorescencia a tiempo real (FLIM) detecta de manera precisa la disfunción mitocondrial en ovocitos de ratón

Objetivo: Determinar como la imagen metabólica mediante el uso de microscopia de fluorescencia a tiempo real (FLIM) identifica diferencias metabólicas entre ovocitos normales y aquellos con disfunción metabólica.

Diseño: Estudio Experimental.

Lugar: laboratorios de investigación académicos.

Pacientes: Ninguno.

Intervenciones: Ovocitos de ratones *knockout* para *Clpp* (peptidasa caseinolítica P; n=52) fueron comparados con ovocitos del grupo salvaje (WT) (n=55) como modelo de disfunción ovocitaria severa. Ovocitos de ratones envejecidos (1 año de edad; n=29) fueron comparados con ovocitos de ratones jóvenes (12 semanas de edad; n=35) como modelo de disfunción ovocitaria leve.

Medida de los resultados principales: FLIM fue empleada para de medir la autofluorescencia natural de la nicotinamida adenina dinucleótido deshidrogenasa (NADH) y de la flavina adenina dinucleótido (FAD) en ovocitos individuales. Se obtuvieron ocho parámetros metabólicos de cada medida (4 por fluoróforo): tiempo de vida de la fluorescencia corta (t1) y larga (t2), intensidad de fluorescencia (I), y fracción de la molécula unida al enzima(F). Niveles de especies reactivas de oxígeno (ROS) y la tasa de desarrollo de blastocisto fueron medidas para valorar la seguridad de la iluminación.

Resultados: Los ovocitos de ratón *Clpp-knockout* en comparación con los WT mostraron, una FAD *t1* y *t2* más largas, *I* más alta, *NADH t2* más larga y *F* más baja. En los ratones envejecidos en comparación con los jóvenes, FAD t1 fue más larga e I más baja, *NADH t1* y *t2* fueron más cortas e *I* y *F* más bajas. FLIM no afectó los niveles de ROS ni la tasa de desarrollo de blastocisto.

Conclusiones: Los parámetros medidos por FLIM muestran una clara diferenciación entre ovocitos *Clpp-knockout* versus *WT*, y entre ovocitos envejecidos versus jóvenes. FLIM podría ser potencialmente utilizado como un método no invasivo para evaluar la función mitocondrial en ovocitos.